JOHANNES KEPLER UNIVERSITY LINZ

Institute of Computational Mathematics

A Unified Stable Space-Time Finite Element Scheme for Non-Newtonian Power Law Models

Ioannis Toulopoulos

Institute of Computational Mathematics, Johannes Kepler University
Altenberger Str. 69, 4040 Linz, Austria

NuMa-Report No. 2021-06 August 2021

Technical Reports before 1998:

1995

95-1	Hedwig Brandstetter *Was ist neu in Fortran 90?*	March 1995
95-2	G. Haase, B. Heise, M. Kuhn, U. Langer *Adaptive Domain Decomposition Methods for Finite and Boundary Element Equations.*	August 1995
95-3	Joachim Schöberl *An Automatic Mesh Generator Using Geometric Rules for Two and Three Space Dimensions.*	August 1995

1996

96-1	Ferdinand Kickinger *Automatic Mesh Generation for 3D Objects.*	February 1996
96-2	Mario Goppold, Gundolf Haase, Bodo Heise und Michael Kuhn *Preprocessing in BE/FE Domain Decomposition Methods.*	February 1996
96-3	Bodo Heise *A Mixed Variational Formulation for 3D Magnetostatics and its Finite Element Discretisation.*	February 1996
96-4	Bodo Heise und Michael Jung *Robust Parallel Newton-Multilevel Methods.*	February 1996
96-5	Ferdinand Kickinger *Algebraic Multigrid for Discrete Elliptic Second Order Problems.*	February 1996
96-6	Bodo Heise *A Mixed Variational Formulation for 3D Magnetostatics and its Finite Element Discretisation.*	May 1996
96-7	Michael Kuhn *Benchmarking for Boundary Element Methods.*	June 1996

1997

97-1	Bodo Heise, Michael Kuhn and Ulrich Langer *A Mixed Variational Formulation for 3D Magnetostatics in the Space $H(rot) \cap H(div)$*	February 1997
97-2	Joachim Schöberl *Robust Multigrid Preconditioning for Parameter Dependent Problems I: The Stokes-type Case.*	June 1997
97-3	Ferdinand Kickinger, Sergei V. Nepomnyaschikh, Ralf Pfau, Joachim Schöberl *Numerical Estimates of Inequalities in $H^{\frac{1}{2}}$.*	August 1997
97-4	Joachim Schöberl *Programmbeschreibung NAOMI 2D und Algebraic Multigrid.*	September 1997

From 1998 to 2008 technical reports were published by SFB013. Please see
`http://www.sfb013.uni-linz.ac.at/index.php?id=reports`
From 2004 on reports were also published by RICAM. Please see
`http://www.ricam.oeaw.ac.at/publications/list/`
For a complete list of NuMa reports see
`http://www.numa.uni-linz.ac.at/Publications/List/`

A unified stable space-time finite element scheme for non-Newtonian power law models.

Ioannis Toulopoulos
Institute of Computational Mathematics,
Johannes Kepler University,
Altenberger Strasse 69 A-4040 Linz Austria
ioannis.toulopoulos@jku.at

Abstract

In this work, a stabilized Space-Time Finite Element (ST-FE) scheme is presented for discretizing time dependent viscous shear-thinning fluid flow models, which exhibit a usual power-law stress strain relation. The whole procedure consists in adding simple streamline-upwind terms for stabilizing the discretization of the associated first order terms in spatial and temporal direction. The original time interval is partitioned into time subintervals, which result in a subdivision of the space-time cylinder into space-time subdomains. Discontinuous Galerkin (DG) techniques are applied for the time discretization between the space-time subdomain interfaces. A stability bound is given for the derived ST-FE scheme. In the last part numerical examples on benchmark problems are presented for testing the efficiency of the proposed method.

Keywords: non-Newtonian shear thinning flows, space-time unified formulations, power law Navier-Stokes models, stabilized space-time finite element discretizations, time discontinuous Galerkin discretizations, numerical solutions for channel flow problems.

MSC 2020: 76A05, 76D05, 76M10, 76M25, 35K65

1 Introduction

Incompressible non-Newtonian fluid flows can appear in many chemical engineering processes involving productions of food, plastics, waxy crude oils, etc, but also in problems coming from biology, physics, bioengineering, etc, [43], [14], [46], [47]. The mathematical models, which have been proposed for describing these type of flows, are mainly Navier-Stokes type systems, where the non-Newtonian flow behavior is usually described by means of a variable viscosity in the constitutive relation, [58], [23]. The most common case is this where the viscosity depends on the magnitude of the shear rate through a p-power law relation, [14], [8], [46]. In the present work such a p-power law Navier-Stokes system (pNS) is considered.

In the past four decades, a huge effort has been devoted for developing efficient numerical methods for non-Newtonian flow models in order to produce accurate simulations. The main difficulties when discretizing these problems are related to the treatment of the nonlinear parts of the equations, i.e., the treatment of the nonlinear first order terms (inertia terms) and the nonlinear relationship between the strain and the stress tensor. Fully discrete schemes are usually derived by applying a finite element discretization coupled with an implicit time integration method, see e.g., [23], [18], [56], [2], [16]. For a more flexible treatment of the nonlinear nature of the problem, operator splitting algorithms have been developed for the time discretization. These approaches allow a decoupling of the original implicit problem, into simpler sub-problems, which are solved in a sequential way, see, [23], [31], [22], [55]. In any case a suitable method must be applied for solving the resulting sub-problems, where usually large time steps can not be used applied due to stability reasons,

[34], [19]. This can reduce the flexibility of the method when extra refined meshes must be used for resolving complex flow features.

Last years ST-FE methods have been proposed for solving time evolution problems, [39]. The key idea is to consider the time variable in the time dependent problem as another spatial variable and the associated time derivative term, lets say $\partial_t \mathbf{u}$, as an advective term in time direction. In view of this, a unified space-time variatioanl formulation is derived, which in turn helps on devising unified finite element discretizations in time and in space. The discretization of time derivative can be stabilized by introducing classical stabilization techniques known from convection dominated problems, [54], [10], [20].

The idea of using finite element techniques for discretizing problems in space and in time simultaneously is not new, and several variants have been analyzed in the past, see e.g., [3], [30], [62], [4], [51], [69], [26], [63], [38], Lately, interesting space-time discretizations, including discontinuous Galerkin (DG) techniques, have been proposed for solving more realistic problems, cf. [59], [60], [57], [61], [33], [32], [27], [67], and the references contained in those works. More recently unified ST discretizations in Isogeometric Analysis framework with continuous in time, [37], [40], and discontinuous in time [29], [41], approaches have been presented.

Although several ST methods have been applied for solving classical Navier Stokes problems, extensions to pINS problems have not been really investigated. The aim of this work is to present a stable discontinuous in time and continuous in space FE discretization for pINS systems, which allows the use of the same class of polynomial spaces for the pressure and the velocity. This is enhanced in the whole discredization by adding appropriate terms into the discrete form of the continuity equation. The background and the construction of the proposed method follow mainly the ideas presented in [59], [27], but there are several differences related to the stability of the scheme, the nonlinear viscosity, the divergence free constraint, the implementation and imposition of the boundary conditions. An advantage of the proposed scheme with respect to the classical approaches mentioned previously, is the possibility to achieve high order discretizations in time avoiding restrictions between the temporal and spatial grid size. The work is an extension of the ST-FE method for parabolic p-Laplacian proposed in [64], to general pINS systems. The numerical shceme is stabilized by adding appropriate Streamline-Upwind terms,[10], [10], [32], [33], consisting of products between the first order derivatives of the unknowns and the test functions. Variations of this approach which can lead to least-squares approaches can be found in [59]. During a procedure of showing an energy stability bound, these products lead to coercive and convex terms, which demonstrates their role in the stabilization of the scheme.

Following DG ideas, the space-time computational domain Q_T is subdivided initially into a group of space-time subdomains (slaps) Q_n, i.e., $\bar{Q}_T = \cup_n \bar{Q}_n$, where every Q_n is discretized into a mesh $\mathcal{T}_h^n$ of tetrahedra (quadrilaterals or hexahedra) mesh elements. On the $\mathcal{T}_h^n$ meshes, we define the associated finite dimensional spaces V_h^n which are used for the discretization of the problem. The basis functions of each V_h^n are continuous within Q_n, but discontinuous in time across the common interfaces of Q_n with Q_{n-1} and Q_{n+1}, see Fig. 1(b). The final space-time discrete problem is solved in a sequential manner with respect to Q_n, i.e., one Q_n at time. The communication of the numerical solution between the subdomain interfaces is achieved by introducing a simple upwind numerical flux coming form the DG methodology, [44]. The whole computational cost can be quite low, because in any case the problem can be solved using large grid steps in time direction and/or using linear polynomial spaces. Note that in case of using tensor product spaces, the proposed approach gives the opportunity of choosing independently high order basis functions in time and in space. This can increase the accuracy of the computations while keeping large grid

steps in time direction. Also the accuracy can be increased by applying anisotropic mesh refinement procedures. Such methods have been applied successfully in several realistic problems, see [60], [61], and the references therein. The overall efficiency of the proposed approach can be further improved when parallel computing environments are used for its materialization, [29],[21], [42]. Anyway after the space-time discretization, we lead to a nonlinear algebraic system which is solved by applying a semi-implicit (Picard) iterative procedure. Due to the singular nature of the stress tensor around the critical points where $\nabla \mathbf{u} = 0$, the use of advanced Newton approaches does not really improve the efficiency, [65], [28]. However, for the numerical examples presented here, the nonlinear solver convergences after seven (maximum) iterative steps.

In the numerical examples, two flow problems in channels are discussed. It is known that channel flows are of interest since they meet in many practical engineering applications, [14]. Usually, during the numerical solution of problems in channels, the physical domain is truncated and artificial inflow and outflow boundaries are introduced in order to define the geometry of the associated computational domain and to focus on the region of interest. On the inflow/outflow boundary parts physical relevant boundary conditions are not (in general) known, and thus artificial boundaries conditions need to be derived. On inflow parts a fully developed profile for the velocity is prescribed. Concerning outflow parts, the derivation of the artificial boundary conditions involves usually a prescription of the normal component of the stress vector, see e.g., [9], [35], [5]. In many applications the estimation of the normal forces is not an easy task, since they depend on the flow features. Often normal force estimations are derived through a well-posed problem analysis and energy estimates, [11], [12], [13]. Nevertheless for unidirectional flows, as these which are studied in the numerical tests, the physics of the flow can help on deriving artificial outflow conditions, [36]. Here, we give an expression of the normal force in terms of the outflow velocity, following an approach which is based on a simple application of the momentum balance equations. Note that a simple imposition of the induced normal force to be zero, (i.e., do-nothing conditions), leads to inappropriate setting for non-Newtonian flow problems, see discussion in [36].

The remaining parts of this work are organized as follows: In Section 2 the power-low Navier-Stokes model for non-Newtonian flow motions is given and the main quantities are described. Section 3 includes the space-time finite element discretization, a stability estimate for the derived method, and the derivation of the artificial outflow boundary conditions. In Section 4, numerical examples are presented, which concern investigations for the asymptotic convergence of the discretization error and to some benchmark selected problems in channels. The paper closes with the conclusions.

2 Problem statement

2.1 Notations

Let Ω be a bounded Lipschitz domain in $\mathbb{R}^d$, $d = 2, ..., 4$, with boundary $\Gamma = \partial\Omega$. Let $1 < p < \infty$ be fixed and ℓ be a non-negative integer. As usual, $L^p(\Omega)$ denotes the Lebesgue space for which $\int_\Omega |\phi(x)|^p \, dx < \infty$, endowed with the norm $\|\phi\|_{L^p(\Omega)} = \big(\int_\Omega |\phi(x)|^p \, dx \big)^{\frac{1}{p}}$, and $W^{\ell,p}(\Omega)$ is the Sobolev space, which consists of functions $\phi : \Omega \to \mathbb{R}$ such that their

weak derivatives up to order ℓ exist and belong to $L^p(\Omega)$. We further define the spaces

$$W_0^{\ell,p}(\Omega) := \{\phi \in W^{\ell,p}(\Omega) \text{ such that } \phi|_{\partial\Omega} = 0\}, \tag{2.1a}$$

$$W_\Gamma^{\ell,p}(\Omega) := \{\phi \in W^{\ell,p}(\Omega) \text{ such that } \phi|_{\Gamma\subset\partial\Omega} = 0\}, \tag{2.1b}$$

$$Q(\Omega) := \{q \in L^{p'}(Q_T), \text{ with } p' = \frac{p}{p-1},\ p > 1\}. \tag{2.1c}$$

The extension of (2.1) to vector functions is denoted by using bold symbols, i.e., $\mathbf{W}^{\ell,p}(\Omega) := \{\boldsymbol{\phi} = (\phi_1, \ldots, \phi_d) \in [W^{1,p}(\Omega)]^d\}$. We refer the reader to [1] for more details about Sobolev spaces.

2.2 The p-power law Navier-Stokes system

In this paragraph the system for describing the motion of an incompressible non-Newtonian fluid with velocity flow $\mathbf{u} = (u, v)$ is given. We consider that the motion evolves in the space-time cylinder $Q_T = I \times \Omega$, where $I = (0, T)$, $T > 0$, is a given time interval, and $\Omega \subset \mathbb{R}^2$, is a bounded domain with smooth boundary $\Gamma := \partial\Omega$. Many constitutive laws have been proposed for modelling non-Newtonian flow motions in different situations, [8], [15], [23] [14]. The most commonly used is this where the extra stress tensor $\mathbf{S}$ has the form, [36],[17], [28],

$$\mathbf{S}(\mathbf{Du}) := 2\mu(\mathbf{Du})\mathbf{D} := 2\mu_0(\kappa + |\mathbf{Du}|)^{p-2}\mathbf{Du}, \tag{2.2}$$

where μ_0 is the dynamic viscocity depending on the Reynolds number Re, $\kappa > 0$ is a given material constant, $p > 1$ is the shear parameter: for $p > 2$ the fluid shows shear-thickening behavior, for $1 < p < 2$ the fluid exhibits shear-thinning properties, and for $p = 2$ the fluid has Newtonian behavior. Also in (2.2), $\mathbf{Du} = \frac{1}{2}(\nabla\mathbf{u} + \nabla\mathbf{u}^T)(:= D_{1\le i,j\le 2}(\mathbf{u}))$ is the tensor of the symmetric gradient of the velocity (strain tensor), and $|\mathbf{Du}| = \left(\sum_{1\le i,j\le 2}(D_{1\le i,j\le 2}(\mathbf{u}))^2\right)^{1/2}$. Having defined $\mathbf{S}(\mathbf{Du})$, the p-Navier-Stokes type system that governs the fluid motion is

$$\mathbf{u}_t - \text{div}\mathbf{S}(\mathbf{Du}) + [\nabla\mathbf{u}]\mathbf{u} + \nabla P = \mathbf{f}, \quad \text{in } Q_T, \tag{2.3a}$$

$$\nabla \cdot \mathbf{u} = 0, \quad \text{in } Q_T, \tag{2.3b}$$

$$\mathbf{u}(0) = \mathbf{u}_0, \quad \text{in } \Omega, \tag{2.3c}$$

$$\tag{2.3d}$$

where the velocity $\mathbf{u}$ and the pressure P are the unknowns, $\mathbf{f}$ is a given external body force vector, and $\mathbf{u}_0$ is a given divergence-free initial condition. The system (2.3) is completed by imposing appropriate boundary conditions. Through this work, we assume that the boundary $\Gamma := \partial\Omega$ consists of three disjoint parts $\Gamma = \Gamma_D \cup \Gamma_0 \cup \Gamma_N$, which remain fixed in time. We set $\Sigma := \Gamma \times I$ the lateral boundary of Q_T, which is subdivided into three parts, $\Sigma_D := \Gamma_D \times I$ (inflow part), $\Sigma_0 := \Gamma_0 \times I$ (solid wall), $\Sigma_N := \Gamma_N \times I$ (outflow part), where the following boundary conditions are imposed

$$\mathbf{u} = \mathbf{u}_D \neq 0, \quad \text{on } \Sigma_D \tag{2.4a}$$

$$\mathbf{u} \cdot \mathbf{n}_{\Sigma_0} = 0, \qquad \text{on } \Sigma_0 \tag{2.4b}$$

$$\left(\mathbf{S} - PI_{2\times 2}\right) \cdot \mathbf{n}_{\Sigma_N} = \mathbf{h}_N, \qquad \text{on } \Sigma_N \qquad , \tag{2.4c}$$

where $\mathbf{u}_D$, and $\mathbf{h}_N$ are given data, and $\mathbf{n}_{(.)}$ is the outer normal to the related boundary part, and $I_{2\times 2}$ is the identity matrix. An illustration is given in Fig. 1(a).

We consider the case where the inflow data $\mathbf{u}_D$ do not vary in time and it holds $\mathbf{u}_D(x) \cdot \mathbf{n}_{\Sigma_D}(x) < 0,\ x \in \Sigma_D$. We further suppose that for all $t \in I$ holds $\mathbf{u}(x) \cdot \mathbf{n}_{\Sigma_N}(x) > 0,\ x \in \Sigma_N$ and $-\int_{\Sigma_D} \mathbf{u}_D \cdot \mathbf{n}_{\Sigma_D} |\mathbf{u}_D|^2\, dS \geq \int_{\Sigma_N} \mathbf{u} \cdot \mathbf{n}_{\Sigma_N} |\mathbf{u}|^2\, dS$. The data $\mathbf{h}_N$ in (2.4c) are in general not known. Below using the conservation of the momentum, we give an estimation of $\mathbf{h}_N$ in terms of the outflow velocity $\mathbf{u}$. For later use we define

$$\begin{aligned} \boldsymbol{\sigma}(\mathbf{u}, P) =& - P\mathbf{I} + 2\mu(\mathbf{Du})\,\mathbf{Du}, \\ \mathbf{F}(\mathbf{Du}) =& (\kappa + |\mathbf{Du}|)^{\frac{p-2}{2}} \mathbf{Du}. \end{aligned} \tag{2.5}$$

We recall the inequalities, [17], [48],

$$\begin{aligned} \mathbf{S}(\mathbf{Du}) : \mathbf{Du} &\geq c_1 |\mathbf{F}(\mathbf{Du})|^2, \\ \|\mathbf{F}(\mathbf{Du})\|_{L^2}^2 &\geq c_2 (\kappa + \|\mathbf{Du}\|_{L^p})^{p-2} \|\mathbf{Du}\|_{L^p}^2, \end{aligned} \tag{2.6}$$

with $c_1 > 0$, $c_2 > 0$ independent of $\mathbf{u}$.

Furthermore, let the vector functions $\mathbf{v} = (v_1, v_2)$ and $\mathbf{w} = (w_1, w_2)$, such that $\mathrm{div}\mathbf{v} = 0$. We recall the identities

$$[\nabla \mathbf{v}]\mathbf{v} \cdot \mathbf{w} = \mathrm{div}(\mathbf{v}\mathbf{v}^\top) \cdot \mathbf{w} - (\mathrm{div}\mathbf{v})\mathbf{v} \cdot \mathbf{w}, \tag{2.7a}$$

$$\int_\Omega \mathrm{div}(\mathbf{v}\mathbf{v}^\top) \cdot \mathbf{v}\, dx - \frac{1}{2} \int_\Omega (\mathrm{div}\mathbf{v})\, (\mathbf{v} \cdot \mathbf{v})\, dx = \frac{1}{2} \int_{\partial\Omega} (\mathbf{v} \cdot \mathbf{n}_{\partial\Omega})\, (\mathbf{v} \cdot \mathbf{v})\, dS, \tag{2.7b}$$

where

$$\mathrm{div}(\mathbf{v}\mathbf{v}^\top) = \begin{pmatrix} \partial_x(v_1 v_1) + \partial_y(v_1 v_2) \\ \partial_x(v_2 v_1) + \partial_y(v_2 v_2) \end{pmatrix}.$$

Weak formulation Suppose that the fluid is filling the domain Q_T and assume that $\mathbf{h}_N = 0$, $\mathbf{u} = 0$ on Σ_0, and $\mathbf{u}_D$, $\mathbf{f}$, $\mathbf{u}_0$ are smooth functions. Using (2.4), the symmetry of $\mathbf{S}$, one can express a variational formulation for (2.3) as,

$$\int_{Q_T} \mathbf{u}_t(x,t) \cdot \boldsymbol{\phi}(x,t) + \mathbf{S}(\mathbf{Du}(x,t)) : \mathbf{D}\boldsymbol{\phi}(x,t) - P(t)\mathrm{div}\boldsymbol{\phi}(x,t) \tag{2.8a}$$

$$+ [\nabla \mathbf{u}(x,t)]\mathbf{u}(x,t) \cdot \boldsymbol{\phi}(x,t)\ dx\, dt = \int_{Q_T} \mathbf{f}(x,t) \cdot \boldsymbol{\phi}(x,t)\ dx\, dt, \tag{2.8b}$$

$$\int_{Q_T} \mathrm{div}\mathbf{u}(t)\, q(t)\ dx\, dt = 0, \tag{2.8c}$$

$$\mathbf{u}(0) = \mathbf{u}_0, \quad \text{with} \quad \mathrm{div}\mathbf{u}_0 = 0, \tag{2.8d}$$

for all $\boldsymbol{\phi} \in \mathbf{W}^{1,p}(Q_T)_{\Sigma_D \cup \Sigma_0}$, $q \in Q(Q_T)$ and $x = (x_1, x_2)$. The problem given in (2.8) is not complete, because conditions under which existence-uniqueness result can be guaranteed, are not provided. Such an investigation is given in [17], [7].

Remark 2.1. *Let the term* $-2\mathrm{div}\mathbf{Du}$*. Multiplying this term with* $\boldsymbol{\phi}$*, performing a component-wise integration by parts in space, and then using the symmetry of* $\mathbf{Du}$*, we obtain*

$$\begin{aligned} (-2\mathrm{div}\mathbf{Du}, \boldsymbol{\phi})_{L^2(Q_T)} =& 2(\mathbf{Du}, \nabla\boldsymbol{\phi})_{L^2(Q_T)} - (2\mathbf{Du} \cdot \mathbf{n}_\Sigma, \boldsymbol{\phi})_{L^2(\Sigma)} \\ =& (\mathbf{Du}, \nabla\boldsymbol{\phi})_{L^2(Q_T)} + (\mathbf{Du}, \nabla\boldsymbol{\phi})_{L^2(Q_T)} - (2\mathbf{Du} \cdot \mathbf{n}_\Sigma, \boldsymbol{\phi})_{L^2(\Sigma)} \\ =& (\mathbf{Du}, \nabla\boldsymbol{\phi})_{L^2(Q_T)} + (\mathbf{Du})^\top, (\nabla\boldsymbol{\phi})^\top)_{L^2(Q_T)} - (2\mathbf{Du} \cdot \mathbf{n}_\Sigma, \boldsymbol{\phi})_{L^2(\Sigma)} \\ =& (\mathbf{Du}, \nabla\boldsymbol{\phi})_{L^2(Q_T)} + (\mathbf{Du}, (\nabla\boldsymbol{\phi})^\top)_{L^2(Q_T)} - (2\mathbf{Du} \cdot \mathbf{n}_\Sigma, \boldsymbol{\phi})_{L^2(\Sigma)} \\ =& 2(\mathbf{Du}, \mathbf{D}\boldsymbol{\phi})_{L^2(Q_T)} - (2\mathbf{Du} \cdot \mathbf{n}_\Sigma, \boldsymbol{\phi})_{L^2(\Sigma)}. \end{aligned} \tag{2.9}$$

Relation (2.9) has been used in the derivation of (2.8a).

3 The space-time finite element approximation

The space-time discretization of (2.8) is based on defining a finite element space over all space-time cylinder Q_T. For this we see the time derivative as an advection term and we derive a unified finite element formulation for discretizing simultaneously in space and time direction. For efficient reasons, DG techniques are used in the time direction. Thus the domain Q_T is described as a union of space-time subdomains Q_n. Hence, the time interval $\bar{I} = [0, T]$ is partitioned into a collection of uniform subintervals $\bar{I}_n = [t_n, t_{n+1}]$, with $0 = t_0 < t_1 < \ldots < t_{N_Q} = T$. The space-time subdomains are defined as $Q_n = I_n \times \Omega$, and $\bar{Q}_T = \cup_n \bar{Q}_n$. The later surface of Q_n is denoted by $\Sigma_{Q_n} := \Gamma \times I_n$, and analogously, we denote $\Sigma_{0,Q_n} := \Gamma_0 \times I_n$, $\Sigma_{D,Q_n} := \Gamma_D \times I_n$, and $\Sigma_{N,Q_n} := \Gamma_N \times I_n$, where the associated BC's (2.4) are imposed, see Fig. 1(b).

For every Q_n, we consider a conforming mesh partition into closed simplices (e.g., tetrahedra) $\mathcal{T}_h^n := \{E^i\}_{i=1,\ldots,M_n}$. The diameter of every $E \in \mathcal{T}_h^n$ is denoted by h_E and we set $h_n := \max_E h_E$. For the computations presented here, the partitions $\mathcal{T}_h^n$ are qusi-unifom, and furthermore $h_n \approx h_{n+1}$. On each $\mathcal{T}_h^n$ we define the finite dimensional spaces,

$$V_h^n := \{\phi_h \in C^0(\bar{Q}_n) : \phi_h|_E \in \mathbb{P}^k(E), \text{ for all } E \in \mathcal{T}_h^n\}, \tag{3.1}$$

$$\mathbf{V}_{\mathbf{u}_D,h}^n := \{\boldsymbol{\phi}_h = (\phi_{1,h}, \phi_{2,h}) \in \left[V_h^n\right]^2 : \boldsymbol{\phi}_h = \mathbf{u}_D \text{ on } \Sigma_{D,Q_n}\}, \tag{3.2}$$

$$\mathbf{V}_{0,h}^n := \{\boldsymbol{\phi}_h = (\phi_{1,h}, \phi_{2,h}) \in \left[V_h^n\right]^2 : \boldsymbol{\phi}_h = 0 \text{ on } \Sigma_{0,Q_n}\}, \tag{3.3}$$

where $\mathbb{P}^k(E)$ denotes the space of polynomials with degree less than or equal to $k \geq 1$. Note that there are no continuity requirements for the spaces V_h^n across the common interfaces $S_{n-1}^n = \partial Q_n \cap \partial Q_{n-1}$ of the space time subdomains.

The space time finite element approximation of (2.8) on every Q_n is expressed: given $\mathbf{u}_h^{n-1}$, find $\mathbf{u}_h^n = (u_h^n, v_h^n) \in \mathbf{V}_{\mathbf{u}_D,h}^n$ and $P_h \in V_h^n$ such that

$$\begin{aligned}
&\int_{Q_n} \left(\mathbf{u}_{h,t}^n + [\nabla \mathbf{u}_h^n]\mathbf{u}_h^n\right) \cdot \boldsymbol{\phi}_h^n \, dx\, dt + \int_{Q_n} \boldsymbol{\sigma}(\mathbf{u}_h^n, P_h^n) : \mathbf{D}\boldsymbol{\phi}_h^n \, dx\, dt \; - \int_{\Sigma_{N,Q_n}} \mathbf{h}_N \cdot \boldsymbol{\phi}_h^n \, dS \\
&\quad + \sum_{E \in \mathcal{T}_h^n} \int_E \tau_h \Big(\mathbf{u}_{h,t}^n + [\nabla \mathbf{u}_h^n]\mathbf{u}_h^n + \nabla P_h\Big)\Big(\boldsymbol{\phi}_{h,t}^n + [\nabla \boldsymbol{\phi}_h^n]\mathbf{u}_h^n + \nabla q_h\Big) \, dx\, dt \qquad (3.4a) \\
&\quad + \int_{S_{n-1}^n} \left(\mathbf{u}_h^n - \mathbf{u}_h^{n-1}\right) \cdot \boldsymbol{\phi}_h^n \, dS = \int_{Q_n} \mathbf{f} \cdot \left(\boldsymbol{\phi}_h^n + \tau_h(\boldsymbol{\phi}_{h,t}^n + [\nabla \boldsymbol{\phi}_h^n]\mathbf{u}_h^n + \nabla q_h)\right) \, dx\, dt, \\
&\quad \int_{Q_n} (q_h + \delta_h \mathrm{div}\boldsymbol{\phi}_h^n)\, \mathrm{div}\mathbf{u}_h^n \, dx\, dt = 0, \quad \forall \boldsymbol{\phi}_h^n \in \mathbf{V}_{0,h}^n, \; q_h \in V_h^n \qquad (3.4b)
\end{aligned}$$

where $\boldsymbol{\sigma}$ has been defined in (2.5), the parameters are $\tau_h = \frac{C_1 h}{(1+|\mathbf{u}_h^n|^2)^{0.5}}$ and $\delta_h = C_2 h$. In the space-time formulation given in (3.4) the approximation spaces are discontinuous in time across the interfaces and the communication of the discrete solution is achieved weakly by introducing the first integral in third line. This discontinuous nature gives some flexibility in memory management and data storage but also helps on a faster performance of the nonlinear solver, compared to the case of using fully continuous polynomial spaces in Q_T. The term $\delta_h \mathrm{div}\, \boldsymbol{\phi}_h^n$ in (3.4b) allows equal order polynomial approximation spaces for $\mathbf{u}_h^n$ and P_h^n. For the case of $k = 1$ we have $\mathrm{div}\boldsymbol{\sigma} = -\nabla P_h^n \mathbf{I}$.

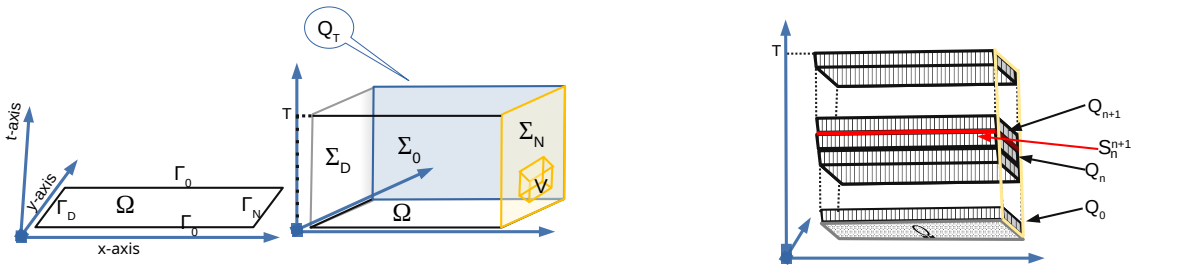

(a) (b)

Figure 1: (a) the space-time computational domain Q_T with the boundary parts, (b) the space-time subdomains Q_n.

A stability estimate for $\mathbf{f} = 0$ and $\boldsymbol{\Gamma}_N = \emptyset$. We consider the terms $\int_{Q_n} \mathbf{u}_{h,t}^n \boldsymbol{\phi}_h^n \, dx\, dt + \int_{S_{n-1}^n} \left(\mathbf{u}_h^n - \mathbf{u}_h^{n-1}\right) \cdot \boldsymbol{\phi}_h^n \, dS$ of (3.4a). Setting $\boldsymbol{\phi}_h^n = \mathbf{u}_h^n$ we have

$$
\begin{aligned}
&\int_{Q_n} \mathbf{u}_{h,t}^n \boldsymbol{u}_h^n \, dx\, dt + \int_{S_{n-1}^n} \left(\mathbf{u}_h^n - \mathbf{u}_h^{n-1}\right) \cdot \boldsymbol{u}_h^n \, dS \\
&= \int_{Q_n} \frac{1}{2} \partial_t (\mathbf{u}_{h,t}^n)^2 \, dx\, dt + \int_{S_{n-1}^n} \left(\mathbf{u}_h^n\right)^2 - \mathbf{u}_h^{n-1} \mathbf{u}_h^n \, dS \\
&= \int_{S_{n-1}^n} \left(\mathbf{u}_h^n\right)^2 - \mathbf{u}_h^{n-1} \mathbf{u}_h^n - \frac{1}{2} (\mathbf{u}_h^n)^2 \, dS + \int_{S_n^{n+1}} \frac{1}{2} \left(\mathbf{u}_h^n\right)^2 dS \\
&= \int_{S_{n-1}^n} \frac{1}{2} \left(\mathbf{u}_h^n\right)^2 - \mathbf{u}_h^{n-1} \mathbf{u}_h^n \, dS + \int_{S_n^{n+1}} \frac{1}{2} \left(\mathbf{u}_h^n\right)^2 dS.
\end{aligned}
\tag{3.5}
$$

Taking the sum over all space-time subdomains Q_n, we get

$$
\begin{aligned}
&\sum_{Q_n} \int_{Q_n} \mathbf{u}_{h,t}^n \boldsymbol{u}_h^n \, dx\, dt + \int_{S_{n-1}^n} \left(\mathbf{u}_h^n - \mathbf{u}_h^{n-1}\right) \cdot \boldsymbol{u}_h^n \, dS \\
&\qquad = \sum_{n=1}^{N} \left\| [[\mathbf{u}_{h,t}^n]] \right\|_{L^2(S_{n-1}^n)}^2 + \left\| [[\mathbf{u}_{h,t}^n]] \right\|_{L^2(S_N)}^2 - \left\| [[\mathbf{u}_{h,t}^n]] \right\|_{L^2(S_0)}^2.
\end{aligned}
\tag{3.6}
$$

Now returning to (3.4a) and using $\mathbf{u}_h^n$, P_h^n as test functions, we have

$$
\begin{aligned}
&\int_{Q_n} \left(\mathbf{u}_{h,t}^n + [\nabla \mathbf{u}_h^n] \mathbf{u}_h^n\right) \cdot \boldsymbol{u}_h^n \, dx\, dt + \int_{Q_n} \mathbf{S}(\mathbf{D}\mathbf{u}_h^n) : \mathbf{D}\boldsymbol{u}_h^n - P_h^n \mathrm{div} \boldsymbol{u}_h^n \, dx\, dt \\
&\quad + \sum_{E \in \mathcal{T}_h^n} \int_E \tau_h \left(\mathbf{u}_{h,t}^n + [\nabla \mathbf{u}_h^n] \mathbf{u}_h^n + \nabla P_h\right)^2 dx\, dt + \int_{S_{n-1}^n} \left(\mathbf{u}_h^n - \mathbf{u}_h^{n-1}\right) \cdot \boldsymbol{u}_h^n \, dS \\
&\quad + \int_{Q_n} (P_h \, \mathrm{div} \boldsymbol{u}_h^n) + \delta_h (\mathrm{div} \boldsymbol{u}_h^n)^2 = 0.
\end{aligned}
\tag{3.7}
$$

Summing over Q_n and using (3.6), (2.6) and the identities (2.7), we find

$$0 < \sum_n \Big\{ \int_{Q_n} c|\mathbf{F}(\mathbf{Du})|^2 \, dx\, dt + \int_{Q_n} \delta_h (\operatorname{div} \boldsymbol{u}_h^n)^2 \, dx\, dt \tag{3.8}$$
$$+ \sum_{E \in \mathcal{T}_h^n} \int_E \tau_h \Big(\mathbf{u}_{h,t}^n + [\nabla \mathbf{u}_h^n] \mathbf{u}_h^n + \nabla P_h \Big)^2 \, dx\, dt \Big\} \leq \big\| [[\mathbf{u}_{h,t}^n]] \big\|_{L^2(S_0)}^2$$
$$- \frac{1}{2} \int_{\Sigma_D} (\mathbf{u}_D \cdot \mathbf{n}_{\Sigma_D}) \, |\mathbf{u}_D|^2 \, dS + \int_{\Sigma_N} (\mathbf{u} \cdot \mathbf{n}_{\Sigma_N}) \, |\mathbf{u}|^2 \, dS,$$

by the assumptions on the problem data and on the boundary conditions.

Prescription of BCs As it has been mentioned above, for flow problems in channels, artificial inflow and outflow boundaries are used for performing the computations. In (2.4) are denoted by Σ_D and Σ_N. The artificial boundary conditions imposed on Σ_N usually include a description of the normal stress, i.e., a suitable form for $\mathbf{h}_N$. Next we will try to give a form of $\mathbf{h}_N$ depending on $\mathbf{u}$, by assuming that there is no backward flow. The derivation is quite straightforward and based on the balance equations of momentum, the same equations which have been used for deriving the Navier-Stokes system (2.3). Note that in this work the density assumed to be fixed $\rho = 1$. We derive the analysis for a small time interval wherein $\partial_t \mathbf{u} \approx 0$ and also suppose $\mathbf{f} = 0$. We consider a reference element V with one face parallel to Γ_{out}, see Fig. 1(a). The momentum flux $\rho\mathbf{u}$ leaving or entering the element V must be fixed.
From the momentum balance for V, the variation of the momentum must be equal to surface forces acting on ∂V, i.e., $\int_V [\nabla \mathbf{u}] \nabla \mathbf{u} \, dx = \int_{\partial V} (\boldsymbol{\sigma} \cdot \mathbf{n}_{\partial V}) \, dS$. Using that $\operatorname{div}\mathbf{u} = 0$ and utilizing the identity $\operatorname{div}(\mathbf{u}\mathbf{u}^\top) = [\nabla \mathbf{u}]\mathbf{u} + \operatorname{div}(\mathbf{u})\mathbf{u}$, we can derive

$$\boldsymbol{\sigma} \cdot \mathbf{n}_{\partial V} = \operatorname{div}(\mathbf{u}\mathbf{u}^\top) \cdot \mathbf{n}_{\partial V} = (\mathbf{u} \cdot \mathbf{n}_{\partial V})\mathbf{u}. \tag{3.9}$$

Since V can be arbitrary small we can consider that (3.9) holds separately for every face of V, or in a different way, the momentum variations in each direction are caused by the surface forces acting in the same direction, and by this we can extract that $\boldsymbol{\sigma} \cdot \mathbf{n}_{out} = (\mathbf{u} \cdot \mathbf{n}_{out})\mathbf{u}$. Thus, returning to (2.4c), we set for the outflow data

$$\mathbf{h}_N = (\mathbf{u} \cdot \mathbf{n}_{out})\mathbf{u}. \tag{3.10}$$

This boundary condition is used in Section Numerical Examples for performing the computations.

4 Numerical Examples

Next the ST-FE scheme (3.4) is used for solving two benchmark problems concerning motions in channels. Also some numerical computations for an academic problem with exact solution are performed, for investigating the asymptotic behavior of a discretization error. In each of the examples linear polynomial spaces are used for every V_h^n space. The parameters are set to be $C_1 = 1.5$ and $C_2 = 0.5$.

Smooth test case- convergence rates The purpose of this example is to investigate the convergence properties of an error related to the discretization in space and the convergence of the L_2 error in time. First a simple steady problem is considered. The flow problem

is defined in $\Omega = \{(x, y) : 0 \leq x \leq 1, 0 \leq y \leq 1\}$ with the space time cylinder $Q_T = I \times \Omega$, $I = (0, T = 50)$. The exact solutions are $(u, v) = ((1 - y)y, 0)$ and $P = 1 - x$. The problem may be viewed as the solution of a fully developed parabolic flow profile between two plates. Based on [17], [7], the error is expressed using the function $\mathbf{F}(\mathbf{D})$ defined in (2.5). Since $\partial_x u = \partial_x v = \partial_y v = 0$, we investigate the asymptotic behavior of the error $e_F = \|\mathbf{F}(\mathbf{D}_{u_y}) - \|\mathbf{F}(\mathbf{D}_{u_{h,y}})\|_{L^2(Q_{N_Q})}$, where $\mathbf{F}(\mathbf{D}_{u_y}) = \begin{bmatrix} 0 & 0.5\partial_y u \\ 0.5\partial_y u & 0 \end{bmatrix}$, and Q_{N_Q} is the final space-time subdomain. The problem is solved on a series of successively refined spatial meshes up to $T = 50$ where the steady solution has been reached. For all spatial meshes the time step mesh is fixed $\Delta t = 0.05$. The first three columns in Table 1 show the convergence rates r_{e_F} of the error e_F for $p \in \{1.2, 1.5\, 1.8\}$. We observe that for all p-test cases the error rates are close to one, and are optimal with respect the polynomial space.

In the next numerical test, the exact solutions are $(u, v) = (e^t(1-y)y, 0)$ and $P = 1-x$. The problem has been solved up to $T = 50$ by applying a mesh refinement only to the time interval by decreasing appropriately the height of the time subdomains. For every refinement step the spatial mesh size is fixed $\Delta h = 0.1$, and each of the time-subdomains include two layers of elements. In the first computation the height of the subdomains is equal to 0.5. The asymptotic convergence behavior of the error $e_{L_2} = \|\partial_t u - \partial_t u_h\|_{L^2}$ is shown in the last three columns in Table 1. It can be observed that for every p-test case the associated rates r_{L^2} are close to the value 0.5. Note that there is no discretization error analysis of the proposed method (3.4).

errors	e_F			$\|\partial_t u - \partial_t u_h\|_{L^2}$		
p:=	p=1.2	p=1.5	p=1.8	p=1.2	p=1.5	p=1.8
$h_0 = 0.5$	Computed rates					
$h_s = \frac{h_0}{2^s}$	r_{e_F}	r_{e_F}	r_{e_F}	r_{L_2}	r_{L_2}	r_{L_2}
$s = 0$	-	-	-	-	-	
$s = 1$	1.00	1.01	1.02	0.35	0.46	0.27
$s = 2$	1.01	1.00	1.00	0.45	0.49	0.41
$s = 3$	0.99	0.998	1.00	0.50	0.54	0.48
$s = 4$	0.93	0.946	0.966	0.54	0.54	0.53
$s = 5$	1.06	1.04	1.068	0.56	0.56	0.56
$s = 6$	1.02	1.02	0.95	0.58	0.57	0.57
$s = 7$	1.02	1.01	1.01	0.58	0.58	0.58

Table 1: Example 1: The convergence rates r_{e_F} and r_{L^2} for all p-test cases.

Flow around a cylinder in an unsteady current The flow of incompressible fluid past over a cylinder, which is located between two plates, is classical benchmark problem and has been studied extensively in the literature, [66], [6], [70], [73, 72]. The geometry is quite simple without singular points. Considering a cylinder with diameter D, the height of the channel is $H = 4D$ and the actual length of the channel is $L = 22D$. The cylinder is placed centrally between the two plates in a distance $1.5D$ from the inflow boundary part Σ_D. An illustration of the geometric set up of the problem is given in Fig. 2(a). The flow presents some complexity. Between the cylinder and the walls is a shear flow, but behind the cylinder and near the upstream axis of symmetry a wake region is formed over a distance depending upon problem characteristics, e.g., blockage ratio ($:= \frac{H}{D}$), Reynolds number Re, etc, [73].

For instance, for $50 < Re \leq 200$, vortex shedding phenomena occur and the wake becomes unstable. More precisely the boundary layer separates due to the adverse pressure

gradient imposed by the divergent geometry, and vortices are created on both rear sides of the cylinder in an alternate manner and then are convected downstream by the flow motion, cf., [71]. Note that a further increase in Re number leads to the question of turbulence and appropriate computational methods are required to solve the problem. The accurate approximation of the stress field and the rest physical quantities near the cylinder and in the wake region are some of the computational tasks for this problem.

For the computations here, the center line of the channel is the $X-axis$, the diameter is $D=1$, and the center of the cylinder is the point $(x=-4, y=0)$. The inflow velocity is $\mathbf{u}_D=(u_D, v_D)=(4-y^2)/4, 0)$. On the outflow boundary part Σ_N the conditions (3.10) are used. In the numerical procedure the wake becomes unstable when a disturbance is introduced. Here during the computations for the the second space-time subdomain we set the velocity on the upper half of the cylinder to be equal to one. The dynamic viscosity μ_0 is defined based on the cylinder diameter D and the maxim inflow velocity $u_{max,D}$, and the Re number, $\mu_0=\frac{u_{max,D}^{3-p}D^{p-1}}{Re}$, where we set $Re=200$. The problem is solved up to final time $T=100$, using $N_Q=400$ space-time subdomains with two layers of mesh elements for each Q_n. The cylinder surface is discretized using 320 mesh elements for capturing the boundary layer phenomena, see Fig. 2(b).

The influence of the power-law index p on the flow pattern has been investigated. Fig 3 shows the streamlines profiles with the contours of the u component for the three values of $p\in\{1.2, 1.5, 1.8\}$ at the final time $T=100$. It can be clearly seen that the flow is unsteady and the vortices formed alternatively on the sides of the cylinder. The wake length appears to increase as p increases from 1.2 to 1.8. Next the time evolutions of the values of v_h component on the point $(x=-2.5, y=0)$ are computed. The results are plotted in Fig 3(a). It can be observed that the values have a periodic behavior which indicates a stable frequency for the vortex shedding. The amplitude is higher for the case $p=1.2$ and decreases for $p=1.5$ and $p=1.8$. Another quantity of interest is the pressure difference between the first stagnation point on the back point on the cylinder surface, i.e., $\Delta P_h=P_h(-4.5, 0, t)-P_h(-3.5, 0, t)$. In Fig. 4(b) the variation of ΔP_h is plotted with respect to time t. For all p-test cases the plots have a periodic behavior. The associated amplitudes and the maximum values of ΔP_h are higher for $p=1.2$ case and decrease as we increase p. The next computations are related to the time evolution of the force that is exerted by the flow on the cylinder surface in the unit direction $\mathbf{e}_x=(1, 0)$, i.e., the drag coefficient C_D, which is defined as $C_D=\frac{-2}{Du_{max,D}^2}\int_{\Gamma_{cyl}}\left(\boldsymbol{\sigma}(\mathbf{u}, P)\mathbf{n}_{\Gamma_{cyl}}\right)\cdot\mathbf{e}_x\, ds$. The variation of C_D with respect to time is given in Fig. 4(c). For the final time steps, e.g., $t>80$, the curves of all p-test cases seems to have the same time period without any oscillations. This shows that the ST-FE scheme remains stable during the last space-time subdomains Q_n. The maximum values of C_D decreases with the increasing value of power law index p. This can be attributed to the reduction of the viscosity as p becomes smaller. Next we compute the values of the viscosity on the barycenter points of the mesh elements which touch the upper surface of the cylinder. The computations concern the final time step. In Fig. 4(d) we plot the associated data. As it is expected the values of the viscosity increase with the increase of p. There exist an oscillatory behavior in the vicinity of the back point of the cylinder. This may be due to the steep changes of the gradient of the velocity at the rear of the cylinder. Lastly it is mentioned that a detailed numerical investigation of this flow problem has been presented in [45], including tests for shear-thickening cases, i.e., $p>2$. The results which have been described above are consistent and in agreement with the results presented in [45].

(a) (b)

Figure 2: Example 2: (a) Illustration of the computational domain, (b) mesh around the cylinder surface, (c) illustration of the successive space-time subdomains.

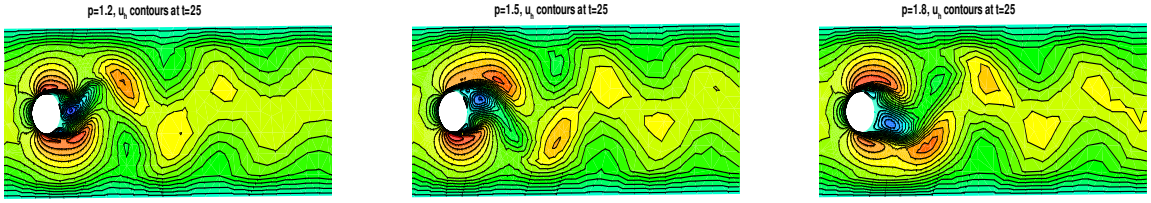

Figure 3: Example 2: The form of the streamlines and the vortex shedding regime, (a) contours of u_h for $p = 1.2$, (b) contours of u_h for $p = 1.5$, (c) contours of u_h for $p = 1.$,

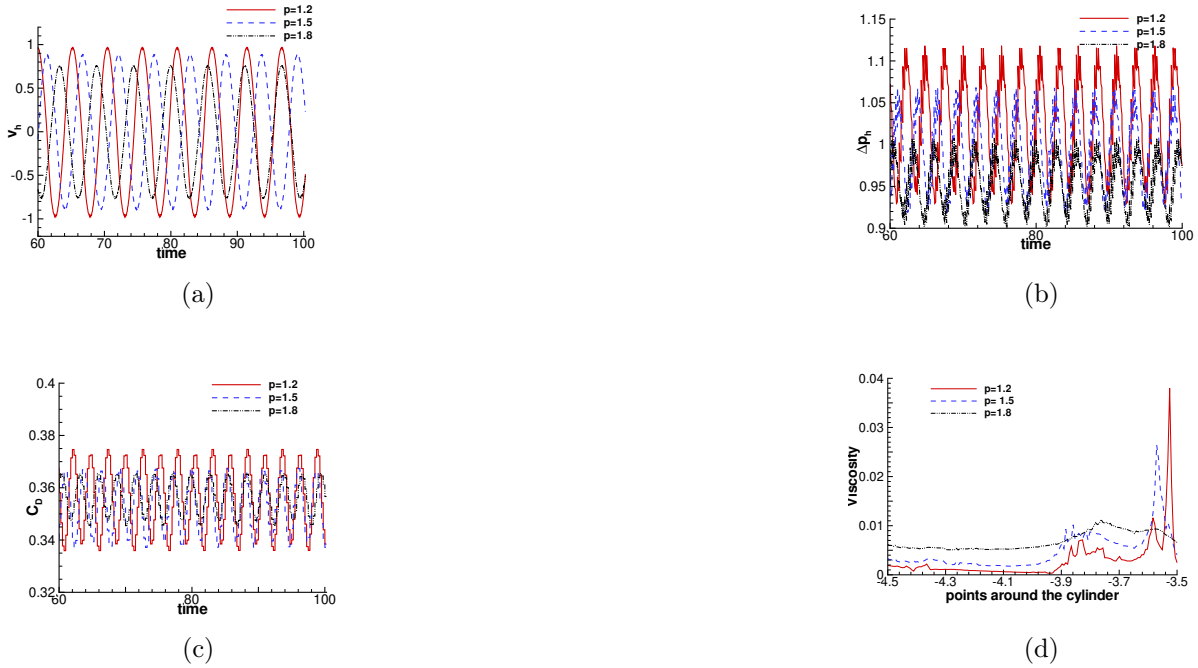

(a) (b)

(c) (d)

Figure 4: Example 2: (a) The periodic behavior of $v_h(-2.5, 0, t)$, (b) The periodic behavior of ΔP_h, (c) The periodic behavior of C_D coefficient, (d) the viscosity around the upper part of the cylinder.

Flow in a constricted channel. In this example the flow in a rigid infinite two dimensional constricted channel is computed. The channel geometry is given in Fig. 5(a), where the flow is from the left to the right. The total channel length is 32 units. The inflow boundary part is located 5 units on the left of the constriction and its half hight is $H = 1$. The maximum height H_C of the constriction is 0.57 and the width L_C is 4.66. The bottom and top walls are placed at $y = -1$ and $y = 1$, respectively. The constriction surface and the channel walls constitute the Σ_0 boundary, where no-slip conditions $(u = 0, v = 0)$ are imposed. At the inflow boundary, a parabolic profile is prescribed, $(u = (1 - y^2), v = 0)$. At the outflow boundary Σ_N the boundary conditions given in (3.10) are used.

In the literature different geometric shapes for the constriction have been proposed depending on particular applications, see [68], [25], [52], [24]. It is known that the height and the width of the constriction affect the flow field structure. The geometry here is similar to this proposed in [49] associated with an arterial stenosis and in [14] associated with rheometer devices for studying blockage effects on non-Newtonian flows.

We note that for sufficiently large numbers, e.g., $Re > 200$, the flow becomes unsteady and vortex shedding and shear layer fluctuations are created. It is not in the purposes of this numerical example to present an investigation in this direction, for details see [25], [53]. However, in the computations below, the viscosity μ_0 is defined by means of the constriction height $\mu_0 = \frac{u_{max,D}^{3-p}(2H_C)^{p-1}}{Re}$, where we set $u_{max,D} = 1$ and $Re = 200$. The problem reaches a steady state where a fully developed Poiseuille profile in the downstream region close to Σ_N boundary is formed.

In order to sufficiently resolve the complex flow features, the mesh density is higher around the constriction region and is decreased in to the rest downstream regions, where the flow is uniform. The spatial mesh size Δh in the constriction region and in the followed area is $\Delta h \approx 0.02$. The problem has been solved up to final time $T = 10$ reaching the steady state. The space time cylinder Q_T is subdivided into $N_Q = 100$ space-time subdomains, where each of them includes two layers of mesh elements. The problem is solved for three power law indices $p \in \{1.2, 1.5, 1.8\}$.

We compute the velocity fields at $T = 10$ and in Figs. 5(b),(c),(d), the contours of the u_h component together with the stream lines are plotted. We observe that for all p-cases the flow field is symmetric with equally sized vortices on either side of the centerline X-axis. The length of the vortices grow with the index p, as well the center of the circulations is found to move downstream with increasing p. Note that this is similar to the planar sudden expansion flow problem, cf. [36]. Anyway, for a better examination in Fig. 5(e), we present the variations of u_h across the X-axis for all p-test cases. Looking carefully the Figs. 5(b),(c),(d), and (e), we observe that the fluid velocity increases in the constriction, with a peak to be present on the centre of the constriction, where the maximum value of u_h increases as the index p increases. Now, moving to the exit of the constriction an adverse pressure gradient happens due to the change of the geometry, which results in flow separation with the two symmetric (with respect to X-axis) recirculation regions close to the walls, as well after the constriction region. After the first recirculation an adverse streamwise pressure gradient occurs, i.e., $\partial P/\partial x < 0$, and a second recirculation region is formed. As it has already pointed out, in the downstream channel area after the wake region, a fully developed Poiseuille flow is formed with a parabolic profile for the u component. Fig. 7 shows the velocity profiles for the points $\{(x, y, t) : x = 28, -1 \leq y \leq 1, t = 100\}$. The velocity profiles for $p = 1.2$ is flatter than those of $p = 1.5$ and $p = 1.8$, as it was expected, because the shear stress near the wall is higher for $p = 1.2$ and this affects the kinematics, see discussion in [36].

Next the pressure P_h fields around the constriction area for the three p cases are shown

in Fig. 6(a),(b),(c). In order to have a better view about the influence of p index to the pressure field, in Fig. 6(d) the associated profiles across the X-axis are compared. Looking the graphs in Fig. 6, we can see that for all p-cases the pressure fields are symmetric with respect to X-axis and show a sharp decreasing in the entrance of the constriction region. The values become minimal at the center of constriction, i.e., at the point $(x - 2.33, y = 0)$. Then moving towards to the downstream points, the values increase having a pick close to the point $(x = 8, y = 0)$ for $p = 1.2$, close to the point $(x = 9, y = 0)$ for $p = 1.5$, and close to $(x = 10, y = 0)$ for $p = 1.8$. The values on these picks are higher for $p = 1.8$ and lower for $p = 1.2$. For the rest points the values exhibit a linear drop which is expected since the flow has a fully developed Poiseuille flow behavior.

For a further validation of the numerical results, a calculation of the forces on the boundary of a fluid element E is performed. The element E has length Δx and its hight extended from $-\Delta y$ to Δy on the X-axis, see Fig. 5(a). Considering fully developed flow (steady-state), then by the momentum equations in x-direction, we can write $\int_{\partial E}(u^2, uv) \cdot \mathbf{n}\, ds = \int_{\partial E}(S_{11} - P, S_{12}) \cdot \mathbf{n}\, ds$. Exploiting the flow characteristics, we can assume that, (i) $v \approx 0$, (ii) u has the same value along the two perpenticular sides of E, (i.e. $\partial_x u \approx 0$), and (iii) $\partial_y P \approx 0$. Now using these simplifications, after few computations, we can find that $2\Delta x S_{12} = 2y(P|_{x=x_0} - P|_{x=x_0+\Delta x})$, see also [36]. Taking the limit as $\Delta x \to 0$, we obtain $S_{12} + y\partial_x P = 0$, for all $t > 0$. Thus, we computed the values of $\sigma := \int_{[t_n,t_{n+1}]} \int_{[-1,1]} (S_{12} + y\partial_x P)\, dydt$ at $x = 28$. In Fig. 7(d), the variations of σ for the last time subdomains are presented. Based on the previous analysis we expect that the values of σ will be close to zero. Indeed, as we can see in Fig. 7(d), the values are less than $4.E-03$ for all p cases and do not increase as the computations approach the final time T. This indicates somehow that the computations reach the steady state and that there are no strong numerical disturbances from the application of the artificial boundary conditions (3.10).

Conclusions

Space-time FE methods have been presented for discretizing p-power law Navier-Stokes type models for incompressible non-Newtonian flows. Continuous FE spaces in spatial direction but discontinuous in time, i.e., across the sub-domain interfaces, have been used. In the numerical scheme an upwind streamline methodology has been introduced for stabilizing the discretization in time, and simple upwind numerical fluxes have been introduced for establishing the communication of the solution between the space-time subdomains. The whole approach has been implemented using linear polynomial basis functions in space and in time, and has been tested in two benchmark problems.

The results look promising to continue with implementations using high-order spaces, possibly discontinuous also in space. The introduction of other type upwind stabilization terms which will be compatible with high-order spaces but without increasing the computational effort it deserves to be investigated. Also new research direction can include combinations of the proposed approach with Domain Decomposition iterative solvers in a parallel environment. A method constructed in this prospective will present increased efficiency and high flexibility in mesh refinement procedures. A work in this direction using an Isogeometric Analysis methodology is in progress.

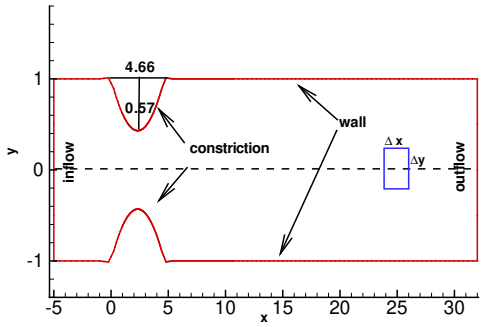

(a)

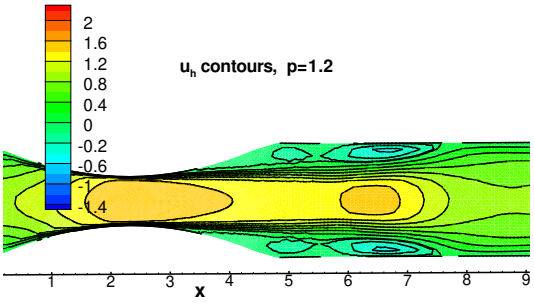

(b)

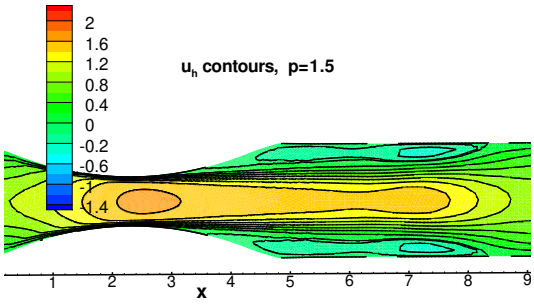

(c)

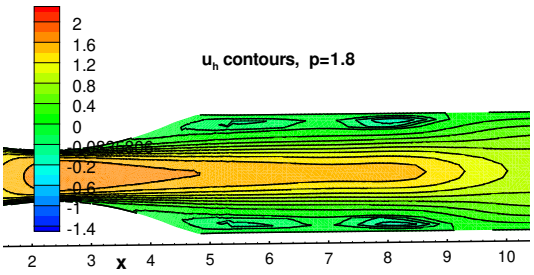

(d)

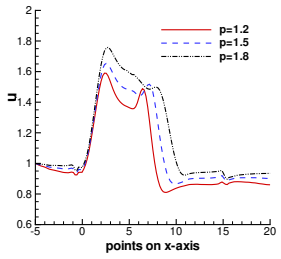

(e)

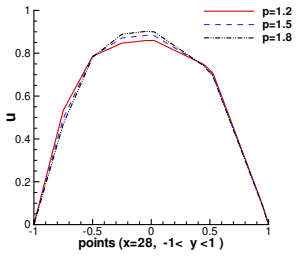

(f)

Figure 5: Example 3: (a) Illustration of the computational domain, (b) u_h and streamlines for $p = 1.2$, (c) u_h and streamlines for $p = 1.5$, (d) u_h and streamlines for $p = 1.8$, (e) u_h variations along x-axis, (f) u_h profiles for the points $\{(x, y, t) : x = 28, -1 \leq y \leq 1, t = 100\}$,

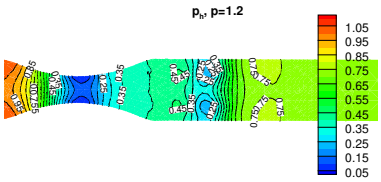

(a)

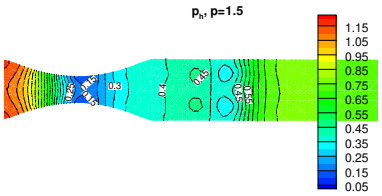

(b)

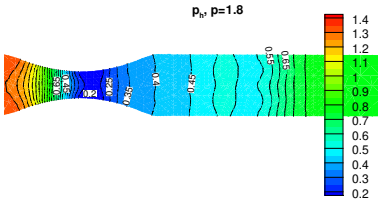

(c)

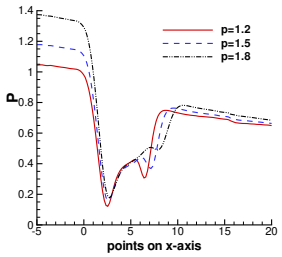

(d)

Figure 6: Example 3: (a) Pressure contours $p = 1.2$, (b) Pressure contours $p = 1.5$, (c) Pressure contours $p = 1.8$, (d) Pressure variations along X-axis

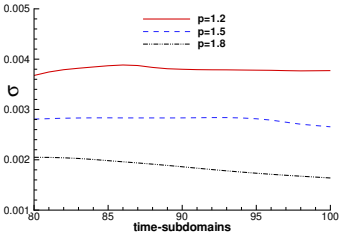

(a)

Figure 7: Example 3: variations of σ for the last time sub-domains.

Acknowledgements

This work has been supported by the JKU-LIT project LIT-2017-4-SEE-004. The author would like to thank the Institute of Computational Mathematics of Johannes Kepler University Linz for hosting this project.

References

[1] R. A. Adams and J. J. F. Fournier. *Sobolev Spaces*, volume 140 of *Pure and Applied Mathematics*. ACADEMIC PRESS-imprint Elsevier Science, second edition, 2003.

[2] A. Aguirre, E. Castillo, M. Cruchaga, R. Codina, and J. Baiges. Stationary and time-dependent numerical approximation of the lid-driven cavity problem for power-law fluid flows at high Reynolds numbers using a stabilized finite element formulation of the VMS type. *Journal of Non-Newtonian Fluid Mechanics*, 257:22–43, 2018.

[3] Randolph E. Bank, Panayot S. Vassilevski, and Ludmil T. Zikatanov. Continuous finite element in space and time for the heat equation. *Mathematics of Computation*, 52(186):255–274, 1989.

[4] Randolph E. Bank, Panayot S. Vassilevski, and Ludmil T. Zikatanov. Arbitrary dimension convectionĄvdiffusion schemes for spaceĄvtime discretizations. *Journal of Computational and Applied Mathematics*, 310:19–31, 2017.

[5] R. Becker, D. Capatina, R. Luce, and D. Trujillo. Finite element formulation of general boundary conditions for incompressible flows. *Computer Methods in Applied Mechanics and Engineering*, 295:240–267, 2015.

[6] M. Behr, D. Hastreiter, S. Mittal, and T.E. Tezduyar. Incompressible flow past a circular cylinder: dependence of the computed flow field on the location of the lateral boundaries. *Computer Methods in Applied Mechanics and Engineering*, 123(1):309–316, 1995.

[7] L. C. Berselli, L. Diening, and M. Růžička. Optimal error estimates for a semi-implicit euler scheme for incompressible fluids with shear dependent viscosities. *SIAM J. NUMER.ANAL*, 47(3):2177– 2202, 2009.

[8] R. B. Bird and R. C. Armstrong amd O. Hassager. *Dynamics of Polymeric Liquids, fluid mechanics*, volume 1. Wiley, New York, 2nd edition, 1987.

[9] F. Boyer and P. Fabrie. Outflow boundary conditions for the incompressible non-homogeneous Navier-Stokes equations. *Discrete and Continuous Dynamical Systems - Series B*, 7(2):pp 219–250, 2007.

[10] A. N. Brooks and T. J.R. Hughes. Streamline upwind/Petrov-Galerkin formulations for convection dominated flows with particular emphasis on the incompressible navier-stokes equations. *Computer Methods in Applied Mechanics and Engineering*, 32(1):199–259, 1982.

[11] Ch.-H. Bruneau. Boundary conditions on artificial frontiers for incompressible and compressible navier-stokes equations. *ESAIM: Mathematical Modelling and Numerical Analysis*, 34(2):303–314, 2000.

[12] Ch.-H. Bruneau and P. Fabrie. Effective downstream boundary-conditions for incompressible Navier-Stokes eguations. *Int. J. Numer. Methods in Fluids*, 19(8):693–705, 1994.

[13] Ch.-H. Bruneau and P. Fabrie. New efficient boundary conditions for incompressible Navier-Stokes equations : a well-posedness result. *ESAIM: M2AN*, 30(7):815–840, 1996.

[14] R. P. Chhabra and J.F. Richardson. *Non-Newtonian Flow and Applied Rheology. Engineering Applications*. Oxford, United Kingdom, 2nd edition, 2008.

[15] D. Cioranescu, V. Girault, and K.R. Rajagopal. *Mechanics and Mathematics of Fluids of the Differential Type*, volume 35 of *Advances in Mechanics and Mathematics*. Springer, Cham, New York, 1 edition, 2016.

[16] M. O. Deville, P.F. Fischer, and E.H. Mund. *High-Order methods ofr Incompressible Fluid Flows*, volume 9 of *Cambridge Monographs on Applied and Computational Mathematics*. Cambridge University Press, Cambridge, U.K.

[17] L. Diening, A. Prohl, and M. Růžička. Semi-implicit euler scheme for generalized newtonian fluids. *SIAM J. NUMER.ANAL*, 44(3):1172 – 1190, 2006.

[18] E. Emmrich. Convergence of a time discretization for a class of non-Newtonian fluid flow. *Communications in Mathematical Sciences*, 6:827–843, 2008.

[19] N. Fiétier and M.O. Deville. Linear stability analysis of time-dependent algorithms with spectral element methods for the simulation of viscoelastic flows. *Journal of Non-Newtonian Fluid Mechanics*, 115(2):157–190, 2003.

[20] L. P. Franca, G. Hauke, and A. Masud. Revisiting stabilized finite element methods for the advective-diffusive equation. *Computer Methods in Applied Mechanics and Engineering*, 195:1560–1572, 2006.

[21] M. Gander. 50 years of time parallel time integration. In T. Carraro, M. Geiger, S. Körkel, and R. Rannacher, editors, *Multiple Shooting and Time Domain Decomposition Methods*, volume 9 of *Contributions in Mathematical and Computational Sciences,*. Springer International Publishing, Cham Heidelberg, 2015.

[22] R. Glowinski and O. Pironneau. Finite element methods for Navier-Stokes equations. *Annu, Rev, Fluid Mech*, 24:167–204, 1992.

[23] R. Glowinski and J. Xu (volume Guest Editors). *Numerical methods for non-Newtonian fluids*, volume XVI of *Handbook of Numerical Analyis*. Springer, Cham, Oxford U.K., 1 edition, 2011.

[24] M. D. GRIFFITH, T. LEWEKE, M. THOMPSON, and K. HOURIGAN. Steady inlet flow in stenotic geometries: Convective and absolute instabilities. *Journal of Fluid Mechanics*, 616:111–133, 2008.

[25] M. D. GRIFFITH, M. C. THOMPSON, T. LEWEKE, K. HOURIGAN, and W. P. ANDERSON. Wake behaviour and instability of flow through a partially blocked channel. *Journal of Fluid Mechanics*, 582:319ĄV340, 2007.

[26] P. Hansbo. Space-time oriented streamline diffusion methods for non-linear conservation laws in one dimension. *Communications in Numerical Methods in Engineering*, 10(3):203–215, 1994.

[27] P. Hansbo and A. Szepessy. A velocity-pressure streamline diffusion finite element method for the incompressible Navier-Stokes equations. *Computer Methods in Applied Mechanics and Engineering*, 84(2):175–192, 1990.

[28] A. Hirn. Finite element approximation of singular power-law systems. *Math. Comp*, 82(283):1247–1268, 2013.

[29] C. Hofer, U. Langer, M. Neumüller, and I. Toulopoulos. Time-multipatch discontinuous Galerkin space-time isogeometric analysis of parabolic evolution problems. *Electronic Transactions on Numerical Analysis.*, 49:126–150, 2018.

[30] T. J.R. Hughes and G. M. Hulbert. Space-time finite element methods for elastodynamics:formulations and error estimates. *Comput. Methods Appl. Mech. Engrg.*, 66:339–363, 1988.

[31] E. J.Dean, R. Glowinski, and T.W. Pan. Operator splitting methods and applications to the direct numerical simulation of particulate flow and to the solution of the elliptic Monge-Ampère equation. In J. Cagnol and J. P. Zolésio, editors, *Control and Boundary Analysis*, pages 1–27. CRC, Boca Ratton, FL), 2005.

[32] C. Johnson. Streamline diffusion finite element methods for incompressible and compressible fluid flow. In B. Engquist, A. Majda, and M. Luskin, editors, *Computational Fluid Dynamics and Reacting Gas Flows*, volume 12 of *The IMA Volumes in Mathematics and Its Applications*. Springer, New York, NY., 1988.

[33] C. Johnson and J. Saranen. Streamline diffusion methods for the incompressible Eulerand Navier-Stokes equations. *Mathematics of Computation*, 47(175):1 – 18, 1986.

[34] R.A. Keiller. Numerical instability of time-dependent flows. *Journal of Non-Newtonian Fluid Mechanics*, 43(2):229–246, 1992.

[35] M. Köhne. *Lp-Theory for Incompressible Newtonian Flows: Energy Preserving Boundary Conditions, Weakly Singular Domains*. Springer Spektrum, Wiesbaden, Germany, 1 edition, 2013.

[36] D. Kröner, M. Růžička, and I. Toulopoulos. Local discontinuous Galerkin numerical solutions of non-Newtonian incompressible flows modeled by p-Navier-Stokes equations. *Journal of Computational Physics*, 270:182 – 202, 2014.

[37] U. Langer, S. E. Moore, and M. Neumüller. SpaceĄvtime isogeometric analysis of parabolic evolution problems. *Computer Methods in Applied Mechanics and Engineering*, 306:342–363, 2016.

[38] U. Langer and A. Schafelner. Adaptive space-time finite element methods for non-autonomous parabolic problems with distributional sources. *Computational Methods in Applied Mathematics*, 20(4):677–693, 2020.

[39] U. Langer and O. Steinbach. *Space-Time Methods: Applications to Partial Differential Equations*, volume 25 of *Radon Series on Computational and Applied Mathematics*. Walter de Gruyter GmbH and Co KG, 2019.

[40] A. Mantzaflaris, F. Scholz, and I. Toulopoulos. Low-rank space-time decoupled isogeometric analysis for parabolic problems with varying coefficients. *Comput. Mathods Appl. Math*, 19(1):123–136, 2019.

[41] S. E. Moore. Space-time multipatch discontinuous galerkin isogeometric Analysis for parabolic evolution problems. *SIAM J. Numer. Anal.,*, 57(3):1471 ĄV 1493, 2019.

[42] B. W. Ong and J. B. Schroder. Applications of time parallelization. *Computing and Visualization in Science*, 23(11):10–25, 2020.

[43] R.G. Owens and T.N. Philips. *Computational Rheology*. Imperial College Press, London, U.K., 2 edition, 2005.

[44] D. A. Di Pietro and A. Ern. *Mathematical Aspects of Discontinuous Galerkin Methods*, volume 69 of *Mathématiques et Applications*. Springer-Verlag Berlin Heidelberg, 2012.

[45] M. K. Rao, A. K. Sahu, and R. P. Chhabra. Effect of confinement on power-law fluid flow past a circular cylinder. *Polymer Engineering and Science*, 51(10):2044–2065, 2011.

[46] M. Rappaz, M. Bellet, and M. Deville. *Numerical Modeling in Materials Science and Engineering*, volume 32 of *Springer Series in Computational Mathematics*. Springer-Verlag, Berlin-Heidelberg, 2003.

[47] A. M. Robertson, A. Sequeira, and R. G. Owens R.G. *Rheological models for blood*, volume 1 of *Cardiovascular Mathematics. Modeling and Simulation of the Cardiovascular System*, pages 211–241. Springer, Berlin Heidelberg.

[48] M. Růžička and L. Diening. Non-Newtonian fluids and function spaces. In *NAFSA 8—Nonlinear analysis, function spaces and applications. Vol. 8*, pages 94–143. Czech. Acad. Sci., Prague, 2007.

[49] S. P. Shupti, M. G. Rabby, and M. M. Molla. Rheological behavior of physiological pulsatile flow through a model arterial stenosis with moving wall. *Hindawi Publishing Corporation, Journal of Fluids*, 2015:1–22, 2015.

[50] D. Song, R. K. Gupta, and R. P. Chhabra. Wall effects on a sphere falling in quiescent power law fluids in cylindrical tubes. *Industrial and Engineering Chemistry Research*, 48(12):5845ĄV5856, 2009.

[51] Olaf Steinbach. Space-time finite element methods for parabolic problems. *Computational Methods in Applied Mathematics*, 15(4):551–566, 2015.

[52] J.S. Stroud, S.A. Berger, and D. Saloner. Influence of stenosis morphology on flow through severely stenotic vessels: implications for plaque rupture. *Journal of Biomechanics*, 33(4):443–455, 2000.

[53] J.S. Stroud, S.A. Berger, and D. Saloner. A pressure-gradient mechanism for vortex shedding in constricted channels. *Physics of fluids*, 25(12):123603– 123630, 2013.

[54] M. Stynes. Steady-state convection-diffusion problems. *Acta Numerica*, 14:445ĄV508, 2005.

[55] R. Sureshkumar, M.D. Smith, R.C. Armstrong, and R.A. Brown. Linear stability and dynamics of viscoelastic flows using time-dependent numerical simulations. *Journal of Non-Newtonian Fluid Mechanics*, 82(1):57–104, 1999.

[56] P. Sváček. On approximation of non-Newtonian fluid flow by the finite element method. *Journal of Computational and Applied Mathematics*, 218:167 – 174, 2008.

[57] K. Takizawa and T. E. Tezduyar. Multiscale space-time fluid structure interaction techniques. *Comput Mech*, 48:247–267, 2011.

[58] R. I. Tanner. *Engineering Rheology*, volume 52 of *Oxford Ebgineering Science Series*. Springer, N.Y., New York, 2 edition, 2000.

[59] T. E. Tezduyar. Stabilized finite element formulations for incompressible flow computations. *Advances in Applied Mechanics*, 28:1–44, 1992.

[60] T. E. Tezduyar and S. Sathe. Modelling of fluidĄvstructure interactions with the spaceĄvtime finite elements: Solution techniques. *International Journal for Numerical Methods in Fluids*, 54(6-8):855–900, 2007.

[61] T. E. Tezduyar and K. Takizawa. Space - time computations in practical engineering applications: a summary of the 25 - year history. *Comput Mech*, 63:747 – 753, 2019.

[62] V. Thomée. *Galerkin Finite Element Methods for Parabolic Problems*, volume 25 of *Springer Series in Computational Mathematics*. Springer-Verlag Berlin Heidelberg, 2nd edition, 2006.

[63] I. Toulopoulos. Space-time finite element methods stabilized using bubble function spaces. *Applicable Analysis*, 99(7):1153–1170, 2018.

[64] I. Toulopoulos. A continuous space-time finite element scheme for quasilinear parabolic problems. *uner review*, Preprint available as JKU-NUMA report: https://www.numa.uni-linz.ac.at/Publications/2021/, 2021.

[65] I. Toulopoulos and T. Wick. Numerical methods for power-law diffusion problems. *SIAM J. Sci. Comput.*, 39(3):A681–A710, 2017.

[66] S. Turek. *Efficient Solvers for Incompressible Flow Problems*, volume 6 of *Lecture Notes in Computational Science and Engineering*. Springer-Verlag, Berlin Heidelberg, 1 edition.

[67] H. van der Ven and J.J.W. van der Vegt. SpaceĄvtime discontinuous galerkin finite element method with dynamic grid motion for inviscid compressible flows: Ii. efficient flux quadrature. *Computer Methods in Applied Mechanics and Engineering*, 191(41):4747–4780, 2002.

[68] A. Van Hirtum, B. Wu, H. Gao, and X.Y. Luo. Constricted channel flow with different cross-section shapes. *European Journal of Mechanics - B/Fluids*, 63:1–8, 2017.

[69] J. Česenek and M. Feistauer. Theory of the space-time discontinuous galerkin method for nonstationary parabolic problems with nonlinear convection and diffusion. *SIAM Journal on Numerical Analysis*, 50(3):1181– 1206, 2012.

[70] J. Volker and M. Gunar. Higher-order finite element discretizations in a benchmark problem for incompressible flows. *International Journal for Numerical Methods in Fluids*, 37(8):885–903, 2001.

[71] C. H. K. Williamson. Oblique and parallel modes of vortex shedding in the wake of a circular cylinder at low reynolds numbers. *Journal of Fluid Mechanics*, 206:579ĄV627, 1989.

[72] M. M. Zdravkovich. *Flow around Circular Cylinders I: Fundamentals*, volume 1 of *Oxford Science Publications*.

[73] M. M. Zdravkovich. *Flow around circular cylinders II: Applications*, volume 2 of *Oxford Science Publications*. Oxford University Press, Oxford, U.K., 2003.

Latest Reports in this series

2009 - 2019

[..]

2020

2020-01	Ioannis Toulopoulos *Viscoplastic Models and Finite Element Schemes for the Hot Rolling Metal Process*	February 2020
2020-02	Rainer Schneckenleitner and Stefan Takacs *Convergence Theory for IETI-DP Solvers for Discontinuous Galerkin Isogeometric Analysis That Is Explicit in h and p*	May 2020
2020-03	Svetoslav Nakov and Ioannis Toulopoulos *Convergence Estimates of Finite Elements for a Class of Quasilinear Elliptic Problems*	May 2020
2020-04	Helmut Gfrerer, Jiří V. Outrata and Jan Valdman *On the Application of the Semismooth* Newton Method to Variational Inequalities of the Second Kind*	July 2020

2021

2020-01	Ioannis Toulopoulos *A Continuous Space-Time Finite Element Scheme for Quasilinear Parabolic Problems*	February 2021
2020-02	Rainer Schneckenleitner and Stefan Takacs *Towards a IETI-DP Solver on Non-Matching Multi-Patch Domains*	March 2021
2020-03	Rainer Schneckenleitner and Stefan Takacs *IETI-DP for Conforming Multi-Patch Isogeometric Analysis in Three Dimensions*	March 2021
2020-04	Ulrich Langer *Adaptive Space-Time Finite Element and Isogeometric Analysis*	March 2021
2021-05	Helmut Gfrerer and Jiří V. Outrata *On Subspaces Contained in Generalized Derivatives and Strong Metric (Sub)regularity*	June 2021
2021-06	Ioannis Toulopoulos *A Unified Stable Space-Time Finite Element Scheme for Non-Newtonian Power Law Models*	August 2021

From 1998 to 2008 reports were published by SFB013. Please see
`http://www.sfb013.uni-linz.ac.at/index.php?id=reports`
From 2004 on reports were also published by RICAM. Please see
`http://www.ricam.oeaw.ac.at/publications/`
For a complete list of NuMa reports see
`http://www.numa.uni-linz.ac.at/Publications/List/`